Intralysosomal Iron Induces Lysosomal Membrane Permeabilization and Cathepsin D–Mediated Cell Death in Trabecular Meshwork Cells Exposed to Oxidative Stress

Yizhi Lin, David L. Epstein, and Paloma B. Liton

Purpose. To investigate the role of intralysosomal redox-active iron in oxidative stress-induced damage in trabecular meshwork (TM) cells.

Methods. Chronic oxidative stress was applied using the hyperoxic model; acute oxidative stress was applied with H_2O_2. Microarray analysis was performed using microarrays. mRNA and protein levels were quantified by real-time PCR and Western blot analysis, respectively. Redox-active iron was monitored using calcein-AM. Apoptosis was quantified using double staining. DNA damage was evaluated by single-cell gel electrophoresis assay. Lysosomal permeabilization was monitored using uptake and acridine orange relocation techniques. Intracellular ROS production was quantified using H_2DCFDA. Cytosolic translocation of cathepsins was visualized with pepstatin-A-BODIPY-FL. Chemical inhibition of cathepsins was achieved with leupeptin and pepstatin A. Silencing of cathepsin expression was accomplished with miRNA sequences. Lysosomal iron chelation was achieved with desferrioxamine.

Results. Chronically stressed TM cells showed elevated levels of redox-active iron and altered expression of genes involved in intracellular iron homeostasis. Although iron increased ROS production and lipofuscin levels and sensitized TM cells to H_2O_2, intralysosomal iron chelation completely protected the cells against H_2O_2-induced cell death and apoptosis. The protective effect of desferrioxamine was mediated by the prevention of lysosomal ROS generation and the rupture of lysosomal membrane, with the subsequent release of cathepsin D into the cytosol.

Conclusions. These results indicate that the generation of intralysosomal ROS induces lysosomal membrane permeabilization and the release of cathepsin D into the cytosol, leading to TM cell death. Here, the authors propose a mechanism by which oxidative stress might contribute to the decrease in cellularity reported in the TM tissue with both aging and disease. (*Invest Ophthalmol Vis Sci.* 2010;51:6483–6495) DOI: 10.1167/iovs.10-5410

Aging of the trabecular meshwork (TM), the tissue responsible for maintaining proper levels of intraocular pressure (IOP), is suspected to be a major risk factor for the development or progression of primary open-angle glaucoma (POAG), a late-onset disease that constitutes the second leading cause of permanent blindness worldwide. Evidence suggests that an acceleration in the production of reactive oxygen species (ROS) causes oxidative damage to the TM with aging[1–5] and that this might contribute to the observed loss in TM tissue functionality in ocular hypertension and in POAG.[6–8] However, the specific mechanisms by which free radicals may exert these pathologic effects on the outflow pathway and the true source of ROS have not yet been determined or even fully hypothesized.

A potential source of intracellular ROS is that generated from H_2O_2 through iron-catalyzed Fenton reactions, which result in the production of highly reactive hydroxyl radicals ($H_2O_2 + Fe^{2+} \rightarrow Fe^{3+} + OH + OH^-$). These newly generated free radicals can induce the peroxidation of adjacent lipids and proteins and oxidative damage to DNA.[9] To meet the physiological demands while avoiding the pro-oxidant effect of iron, cells and organisms handle iron with extreme caution and efficiently prevent free iron from reacting with H_2O_2 by sequestering it within a series of proteins that control either iron uptake (transferrin; transferrin receptor [TFRC]), iron storage (ferritin, composed of ferritin heavy chain [FTH]; and ferritin light chain [FTL]), or iron export (ferroportin [SLC-40]; ceruloplasmin [CP]). Moreover, transferrin-mediated iron uptake and iron storage in ferritin are events controlled by the concentration of free redox-active iron (labile iron pool [LIP]) through the coordinated action of cytosolic iron regulatory proteins (IRPs), which bind to iron-responsive element (IRE) motifs present in the untranslated regions of TFRC and FTH/FTL genes. Thus, a reduction in intracellular iron availability causes IRPs to bind the IRE motifs in the mRNAs of TFRC or FTH/FTL, thereby inhibiting the translation of ferritin and stabilizing the TFRC mRNA to favor iron uptake and decrease storage. In contrast, under high iron concentrations, IRPs are either assembled into clusters or degraded by the proteolytic systems and cannot bind IRE motifs. This situation results in an upregulation of ferritin synthesis and an increase of TFRC mRNA degradation, thus promoting iron storage and inhibiting iron uptake.[10–12]

Intracellular iron levels have been reported to increase exponentially in cultured primary human fibroblasts and in umbilical vein endothelial cells as a function of cellular senescence.[13,14] Similarly, localized iron dysregulation with consequent iron accumulation has been demonstrated to occur in a variety of tissues and species during normal aging.[15–22] It has been postulated that such deposition of iron might contribute to the increased oxidative stress and cellular dysfunction associated with normal aging and with the pathology of a growing number of age-related diseases, including Alzheimer's disease, Parkinson's disease, type 2 diabetes, cardiovascular diseases, and macular degeneration.[16,20,22–25]

From the Department of Ophthalmology, Duke University Eye Center, Durham, North Carolina.

Supported by National Institutes of Health/National Eye Institute Grants R21EY019137, ARRA R21EY019137S, and P30EY005722 and by Research to Prevent Blindness.

Submitted for publication February 19, 2010; revised May 25, 2010; accepted June 15, 2010.

Disclosure: **Y. Lin**, None; **D.L. Epstein**, None; **P.B. Liton**, None

Corresponding author: Paloma B. Liton, Duke University Eye Center, AERI Building, Office 4004, Erwin Road, Box 3802, Durham, NC 27713; paloma.liton@duke.edu.

Although the mechanisms by which iron accumulates intracellularly during aging are still largely unknown, lysosomes have been suggested to play a major role in the intracellular regulation and homeostasis of iron metabolism.[26–28] Lysosomes are the main cellular organelles responsible for the degradation of organelles and long-lived proteins and of extracellular and membrane-bound material. Because of the breakdown of iron-containing endocytosed and autophagocytosed material, significant concentrations of labile iron accumulate within the lysosomes,[15,29] where it participates in Fenton reactions, leading to the generation of lysosomal ROS.

Our laboratory recently reported that prolonged exposure of TM primary cultures to a hyperoxic environment, as an in vitro model of aging, led to a striking increase in ROS production. This increase in iROS production was accompanied by alterations in the lysosomal pathway in the stressed cultures.[30] The purposes of this study were to evaluate the effect of oxidative stress in intracellular iron homeostasis in TM cells and the potential role of intralysosomal iron in outflow pathway pathophysiology. The data presented here provide evidence for an accumulation of redox active iron in TM cells exposed to chronic oxidative stress. Furthermore, we propose a mechanism by which iron-catalyzed oxidative damage might contribute to the decrease in cellularity reported in the TM tissue with both aging and disease.

Materials and Methods

Reagents

Calcein-acetoxymethyl ester (calcein-AM), desferoxamine (DFO), ferric ammonium citrate (FAC), leupeptin, pepstatin A, and H_2O_2 were obtained from Sigma-Aldrich (St. Louis, MO). Salicylaldehyde isonicotinoyl hydrazone (SIH) was kindly provided by Katherine J. Franz (Department of Chemistry, Duke University).

Cell Culture

Primary cultures of porcine and human TM cells were prepared and maintained as previously described.[30] The protocols involving the use of human tissue were consistent with the tenets of the Declaration of Helsinki. The transformed glaucomatous human cell line (GTM-3) and the transformed nonglaucomatous human cell line (NTM-5) were kindly provided by Alcon Research (Fort Worth, TX).[31]

Experimental Model for Chronic Oxidative Stress in PTM cells

Chronic oxidative stress was induced by subjecting TM cells to normobaric hyperoxia conditions as previously described.[30] For this, confluent cultures of TM cells at passage four were grown for 2 weeks at 40% O_2 and 5% CO_2. Control cultures were grown under physiological oxygen conditions (5% O_2, 5% CO_2) in a triple gas incubator.[32]

Microarray Analysis

Total RNA (10 μg) from three independent human TM primary cultures grown under 5% O_2 or 40% O_2 atmosphere were independently hybridized to microarrays (Human Genome U133 Plus 2.0; Affymetrix, Santa Clara, CA) according to the manufacturer's instructions. Data analysis was performed using microarray data analysis software (GeneSpring version 7.0; Silicon Genetics, Redwood City, CA). Raw data from the six hybridizations were normalized to the 50th percentile per chip and to the median per gene. Genes with a differential gene expression were selected and then filtered on flags to retain the genes that were presented in at least one of the conditions. Because some genes were represented in the arrays in more than one spot, we verified a consistent differential expression in all the spots to eliminate false positives.

Quantitative Real-time PCR

Total RNA from TM primary cultures was isolated with a purification kit (RNeasy; Qiagen, Valencia, CA) in accordance with the manufacturer's protocol and were treated with DNase I. RNA yields were determined using a fluorescent dye (RiboGreen; Molecular Probes, Eugene, OR). First-strand cDNA was synthesized from total RNA (1 g) by reverse transcription using oligo(dT) primer and reverse transcriptase (Superscript II; Invitrogen, Carlsbad, CA). Real-time PCR was performed as previously described.[30] The fluorescence threshold value (Ct) was calculated by real-time PCR detection (iCycler iQ; Bio-Rad, Hercules, CA). β-Actin served as an internal standard of mRNA expression. Fold change was calculated using the formula $2^{-\Delta\Delta Ct}$, where $\Delta Ct = Ct_{gene} - Ct_{Act}$, and $\Delta\Delta Ct = \Delta Ct_{Exp} - \Delta Ct_{Con}$. Primer sequences used for the amplifications are shown in Table 1.

Western Blot Analysis

Cells were washed in PBS and lysed in 20 mM HEPES, 2 mM EGTA, 5 mM EDTA, and 0.5% NP-40 containing Halt Protease Inhibitor Cocktail and Halt Phosphatase Inhibitor Cocktail (Pierce, Rockford, IL). Protein concentration was determined with a protein assay kit (Micro BCA; Pierce). Protein samples (10–20 g) were separated by 10% SDS-PAGE and transferred to a polyvinylidene difluoride membrane (Bio-Rad). Membranes were blocked with 5% nonfat dry milk and incubated overnight with anti-ferritin L (SC-14422), anti-cathepsin D (SC-6494), or anti-tubulin (SC-9935) (Santa Cruz Biotechnology, Santa Cruz, CA) or anti-cathepsin B (ab58802–100) from Abcam (Cambridge, MA). Bands were detected by incubation with a secondary antibody conjugated to horseradish peroxidase and chemiluminescence substrate (ECL Plus; GE Healthcare, Pittsburgh, PA).

Measurement of Intracellular Labile Iron Pool

Levels of the cytosolic chelatable iron pool were assayed using calcein-AM, a fluorescent iron-sensitive probe.[33] For this, cells were washed and incubated with 0.15 M calcein-AM for 10 minutes at 37°C in PBS containing 1 mg/mL BSA and 20 mM HEPES, pH 7.3. After calcein loading, cells were trypsinized, washed, and resuspended in this buffer without calcein-AM. Calcein fluorescence was monitored in a fluorescence spectrophotometer (excitation, 488 nm; emission, 518 nm). Once the signal was stable, SIH (100 μM) was added to the reaction, and the increase in calcein fluorescence that resulted from the release of iron from the calcein was recorded.

Quantification of Lipofuscin Content

Endogenous cellular autofluorescence was quantified by flow cytometry (FACSCalibur; BD Biosciences, San Jose, CA). For this, the fluores-

Table 1. Primer Sequences Used for qPCR

Gene Name	Gene Symbol	Forward	Reverse
Ferritin light chain	*FTL*	TTCGGAGCGTCTCTTGAAA	TTCCATAGCGTCCTGGGT
Ferritin heavy chain	*FTH*	CTGCTGGAACTGCACAAACT	CCCAATTCTTTGATGGCTTT
Transferrin receptor	*TFRC*	CACACCTGGATTCCCTTCTT	TGGAAATTGTTTGCACAGGT
Metallothionein 1A	*MT1A*	CACCTCCTGCAAGAAGAGC	CACAGCAGCTGCACTTGTC
Ceruloplasmin	*CP*	GTCCTGGAAAGGAAGACAGC	ATGAGCCCTGAGGCAATATC
Ferroportin	*SLC-40*	GTCATCTTGGCTCCAAATCC	GGCAAATCGGAAATACATGA

cence emitted by 10,000 cells in the FL-2 channel (563- to 607-nm wavelength band) was recorded and analyzed (CellQuest software; BD Biosciences, San Jose, CA).

Quantification of Intracellular ROS Production

Intracellular ROS production was quantified using the cell-permeant ROS indicator 2′,7′-dichlorodihydrofluorescein diacetate (H_2DCFDA; Invitrogen). Briefly, cells (1×10^6) were trypsinized and incubated in 1 mL PBS containing 20 M H_2DCFDA for 30 minutes. After this loading period, cells were washed, and the mean green fluorescence of 10,000 cells was immediately recorded and quantified by flow cytometry (FL-1 channel; CellQuest software; BD Biosciences). Nonstained control cells were included to evaluate baseline fluorescence.

Cell Viability and Cytotoxicity

Cell viability and cytotoxicity were quantified with a cytotoxicity assay (MultiTox-Fluor Multiplex Cytotoxicity Assay; Promega, Madison, WI) that simultaneously measures the relative number of live and dead cells in cell populations. Because of chemical interference, in experiments involving the silencing of cathepsin proteases a cytotoxicity assay (CytoTox 96 Non-Radioactive Cytotoxicity Assay; Promega) that measures the lactate dehydrogenase (LDH) release on cell lysis was used instead. In both cases, assays were performed in accordance with the manufacturer's instructions.

Quantification of Apoptosis and Necrosis

Apoptosis and necrosis were evaluated using YO-PRO-1/propidium iodide (PI) double staining (Vybrant Apoptosis Assay Kit #4; Invitrogen) according to the manufacturer's protocol. Briefly, cells were harvested, washed, and resuspended in cold PBS with suggested dilutions of YO-PRO-1 and PI dyes. Cells were incubated for 30 minutes on ice and then analyzed by flow cytometry (FL1 and FL3 channels). Viable cells exclude both dyes and are YOPRO-1^-/PI^-. Cells in early apoptosis showed increased permeability to YO-PRO-1 and remained impermeable to PI (YO-PRO-1^+/PI), whereas cells in the late phase of apoptosis or those undergoing necrosis were permeable to both dyes (YO-PRO-1^+/PI^+).

Quantification of DNA Damage

DNA fragmentation associated with oxidative DNA damage was analyzed using the single-cell gel electrophoresis assay (Comet Assay Kit; Trevigen, Gaithersburg, MD) in accordance with the manufacturer's instructions. Briefly, 1×10^5 cells were mixed with low melting agarose at 37°C, pipetted onto slides (CometSlides; Trevigen), and maintained at 4°C in the dark for 30 minutes. Slides were immersed in cold lysing solution for 30 minutes at 4°C and then in fresh alkaline electrophoresis solution, pH >13 (300 mM NaOH, 1 mM EDTA) for 30 minutes at room temperature to allow the unwinding of the DNA and the expression of alkali-labile damage. Electrophoresis was conducted at 1 V/cm for 30 minutes (300 mA). After electrophoresis, DNA was stained with SYBR Green and comets were visualized under the fluorescence microscopy. The comet length of 50 randomly selected cells from each group was quantified by a masked observer using comet scoring software (Comet Score; TriTek Corporation, Sumerduck, VA).

Lysosomal Membrane Stability Assay

Lysosomal stability was assayed using probe (Lysotracker [LTR] Invitrogen) uptake and acridine orange (AO) relocation methods. For the LTR uptake method, cells were treated for 3 hours with H_2O_2 (0.5 mM, 0.75 mM) and then were loaded for 15 minutes at 37°C with LTR (500 nM). After the loading period, cultures were washed, and cells with a decreased number of intact lysosomes (pale cells) were detected by their diminished punctuated red fluorescence under the confocal microscopy and were quantified by flow cytometry in the FL3 channel.

For the AO-relocation technique, cells were preloaded with AO (5 μg/mL) for 15 minutes in complete culture medium, rinsed, and then exposed to H_2O_2 (0.5 mM, 0.75 mM) for 1 to 2 hours. The increase in green fluorescence due to the release of AO from ruptured lysosomes was monitored under fluorescence microscopy and quantified by flow cytometry in the FL1 channel.

Translocation of Lysosomal Enzymes

Translocation of cathepsin D (CTSD) to the cytosol was visualized using pepstatin A BODIPY FL (Invitrogen). For this, cells grown in gelatin-coated coverslips were loaded with pepstatin A BODIPY FL (1 μM) and were exposed to H_2O_2 for 1 hour. Pepstatin A BODIPY FL-CTSD complexes were visualized under confocal microscopy.

Construction of pcDNA-GFP-miR-CTSB and pcDNA-GFP-miR-CTSD

Silencing of CTSD and cathepsin B (CTSB) was achieved (BLOCK-iT Pol II miR RNAi System; Invitrogen). For this, microRNA sequences to specifically target porcine CTSB (ACGGCCGGACACAATTTCTAC; GenBank accession no. ef095956) and porcine CTSD (GCCCTGTAATTCTGCGTTGTT; GenBank accession no. NM_001037721) were designed using the online tool (BLOCK-iT RNAi Designer Invitrogen). Pre-miRNA double-stranded oligos were generated by annealing two single-stranded DNA oligonucleotides: the top strand oligo, containing a 5′-overhang region complementary to the cloning vector (TGCTG), the antisense target sequence, the internal loop sequence (GTTTTGGCCACTGACTGAC), and the nucleotides 1 to 8 and 11 to 21 of sense target sequence; and the bottom strand oligo, containing a 5′-overhang region (CCTG) and the reverse complement of the top strand oligo sequence minus 5′-overhang. The obtained pre-miRNAs were then cloned into the expression vector pcDNA 6.2-GW/EmGFP-miR to yield pcDNA-GFP-miR-CTSB and pcDNA-GFP-miR-CTSD. Proper orientation and sequence were confirmed by sequencing. Control plasmid (pcDNA6.2-GW/EmGFP-miR-neg; Invitrogen) was used as a negative control.

Amaxa Nucleofector Transfection

Transfection of primary cultures of porcine TM cells was performed by electroporation (Nucleofector System, T23 program; Amaxa Inc., Gaithersburg, MD) using a kit for primary endothelial cells (Basic Nucleofector Kit; Amaxa Inc.), according to the manufacturer's instructions.

Statistical Analysis

All experimental procedures were repeated at least three times in independent experiments using different cell lines. The percentage of increase of the experimental conditions compared with the control was calculated and averaged. Data are represented as mean ± SD. Statistical significance was calculated using Student's *t*-test for two-group comparisons and one-way or two-way ANOVA for multiple group comparisons (Prism; GraphPad, San Diego, CA). $P < 5\%$ was considered statistically significant.

Results

Altered Iron Homeostasis in GTM Cells and in Primary Cultures of TM Cells Subjected to Chronic Oxidative Stress

To test the potential effects of aging on intracellular iron homeostasis in TM cells, we quantified the mRNA levels of TFRC, FTH, and FTL in primary cultures of porcine TM cells exposed to the experimental model of aging previously described (40% O_2 vs. physiological 5% O_2).[30] Quantitative real-time PCR analysis demonstrated altered mRNA levels of TFRC (1.85 ± 0.25-fold), FTH (2.01 ± 0.16-fold), and FTL (2.44 ±

1.01-fold) with chronic oxidative stress (Fig. 1A). Cells exposed to 40% O_2 also showed decreased mRNA levels of CP (0.47 ± 0.1-fold), a gene involved in iron export with downregulated expression in the glaucomatous outflow pathway.[34] In addition, we observed a significant upregulation (6.09 ± 2.00-fold) of MT1A, a metal-binding protein that has recently been reported to protect macrophages against oxidative stress-induced lysosomal destabilization.[35] Western blot analysis of whole cell lysates using a specific antibody against FTL demonstrated the increased expression of this protein in the cultures exposed to chronic oxidative stress (Fig. 1B).

As shown in Table 2, microarray analysis of human TM cells exposed to a hyperoxic environment also showed altered expression of several genes involved in intracellular iron homeostasis, including IRP1, FTH, PIR, TFRC, and MT1P3 (Table 2), indicating that the dysregulation of iron homeostasis in TM cells with oxidative stress was not species specific. Moreover, qPCR analysis demonstrated the statistically significant upregulation of FTL (1.88 ± 0.23-fold; $P = 0.0028$; $n = 3$) in the immortalized glaucomatous cell line GTM-3 compared with the nonglaucomatous cell line NTM-5 (Fig. 1C). Although it did not reach statistical significance, GTM cells also demonstrated slightly decreased levels of CP (0.5 ± 0.04; $P = 0.063$; $n = 3$). Altogether, these data indicate altered iron homeostasis in TM cells with oxidative stress.

Increased LIP in Primary Cultures of Aging TM cells

Because, as explained in the Introduction, the expression of genes involved in iron homeostasis is controlled by cellular iron content, our data suggested the presence of higher concentrations of free iron in the stressed cultures compared with the nonstressed cultures. To confirm this, we quantified the intracellular LIP using the calcein-AM assay. Calcein-AM is a nonfluorescent lipophilic ester that easily penetrates cell membranes and is intracellularly cleaved by nonspecific cellular esterases into calcein, a fluorescent, nonpermeable compound that is retained within the cell. Calcein-loaded cells show a fluorescence component (ΔF) that is quenched by intracellular free iron. On addition of the cell-permeable iron chelator SIH, iron is released from calcein, which regains its fluorescence. The increase in calcein fluorescence is proportional to the size of the intracellular LIP.[33] As shown in Figure 1D, porcine TM cells grown at 40% O_2 displayed lower calcein fluorescence levels than cells grown at 5% O_2 (185.47 ± 70.36 RFU vs. 341.47 ± 67.71 RFU; $P = 0.0005$; $n = 7$). This decrease in the levels of calcein fluorescence was not caused by the release of the compound due to plasma membrane permeabilization, as demonstrated by Trypan blue staining (data not shown). In addition, calcein fluorescence was recovered on the addition of SIH (100 μM). Moreover, calcein-mediated fluorescence

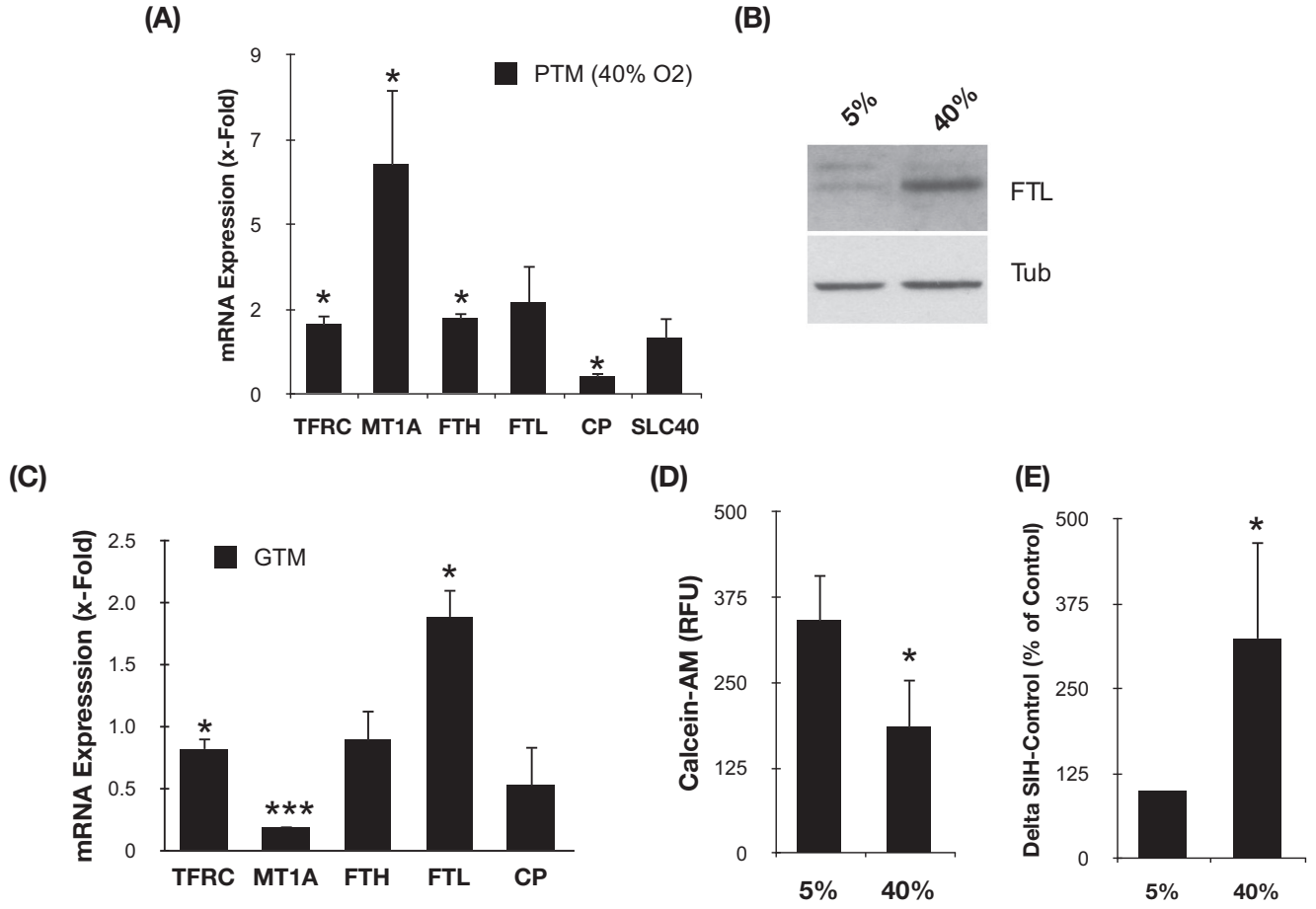

Figure 1. (**A**) Relative mRNA expression levels of genes involved in intracellular iron homeostasis in confluent porcine primary cultures grown for 2 weeks at 40% O_2 compared with 5% O_2 quantified by qPCR. (**B**) Protein levels of FTL assayed by Western blot analysis. (**C**) Relative mRNA expression levels of genes involved in intracellular iron homeostasis in GTM-3 compared with NTM-5 quantified by qPCR. (**D**) Intracellular calcein-induced fluorescence levels in primary cultures of porcine TM cells grown at 5% O_2 and 40% O_2 atmosphere. (**E**) Percentage of increase in calcein-induced fluorescence after addition of SIH. Values represent mean ± SD. $^*P < 0.05$; $^{***}P < 0.001$.

TABLE 2. Expression Levels of Genes Involved in Iron Homeostasis in Human TM Cells Exposed to Chronic Oxidative Stress

Gene Name	Gene Symbol	Unigene	Fold (Mean ± SD)	*P*
Aconitase 1, soluble	*ACO1*	Hs.567229	1.48 ± 0.02	0.0003
Aconitase 2, mitochondrial	*ACO2*	Hs.567229	1.08 ± 0.05	0.0601
Ferritin, heavy polypeptide 1	*FTH*	Hs.524910	1.90 ± 0.65	0.0692
Ferritin, mitochondrial	*FTHP1*	Hs.453583	1.33 ± 0.22	0.0658
Ferritin, light polypeptide	*FTI*	Hs.524910	1.34 ± 0.16	0.0352
Iron-responsive element binding protein 2	*IREB2*	Hs.436031	1.28 ± 0.17	0.0597
Metal response element binding transcription factor 2	*MTF2*	Hs.696220	0.66 ± 0.03	0.0021
Metal-regulatory transcription factor 1	*MTF1*	Hs.436031	0.97 ± 0.21	0.4141
Metallothionein 1 pseudogene 3	*MT1P3*	Hs.696220	1.67 ± 0.19	0.0137
Metallothionein 2A	*MT2A*	Hs.655199	1.12 ± 0.16	0.1697
Pirin (iron-binding nuclear protein)	*PIR*	Hs.655199	1.95 ± 0.18	0.0063
Transferrin receptor (p90, CD71)	*TFRC*	Hs.529618	1.63 ± 0.38	0.0536

increased in higher proportions in the stressed cultures after addition of the iron chelator SIH (Fig. 1E; 324.5% ± 143.73%; $P = 0.01$; $n = 7$), indicating that elevated amounts of Fe^{2+} were displaced from calcein-Fe complexes compared with control. Altogether, these data indicate an increase in redox active iron content in aging cultured porcine TM cells.

Exogenous Iron Increases Lipofuscin Levels and iROS Production and Sensitizes Porcine TM Cells to H_2O_2-Induced Cell Death

We next wanted to investigate whether this increase in iron content in the stressed cultures could be at least partly responsible for the previously reported increase in iROS production and lipofuscin content in TM cells exposed under 40% O_2.[30] For this purpose, we experimentally increased intracellular iron content by incubating porcine TM cells with increasing concentrations of FAC for 3 days. As expected, the addition of FAC to the culture media resulted in a dosage-dependent increase in FTL (up to 10.25 ± 1.50-fold with 1 mM FAC; $P = 0.008$; $n = 3$) and FTH (up to 4.15 ± 1.59-fold with 1 mM FAC; $P = 0.07$; $n = 3$) mRNA levels and a decline in the TFRC mRNA levels (up to 1.38 ± 0.06-fold; $P = 0.008$; $n = 3$) in response to iron treatment (Fig. 2A). Western blot analysis also demonstrated the induction of FTL expression by FAC in a dosage-dependent manner (Fig. 2B), thus confirming an elevation in the intracellular iron content in these cultures. As shown in Figure 3A, FAC-treated cultures displayed higher levels of cellular autofluorescence, which represented peroxidized lipids and protein, compared with the nontreated cultures (ANOVA; $P = 0.0134$; $n = 3$). Such increase was observed even at the lowest FAC dosage (0.01 mM FAC; 237.2% ± 67.2%; $P < 0.05$; $n = 3$) and did not significantly vary with higher FAC concentrations.

To investigate the participation of intracellular iron in Fenton reactions, we measured iROS production in FAC-treated cultures exposed for 1 hour to a bolus dosage of H_2O_2 (0 mM, 0.5 mM, or 0.75 mM). The presence of intracellular iron significantly induced both the constitution (302.99% ± 33.49%; $P < 0.002$; $n = 3$) and the formation of iROS induced by H_2O_2 (456.81% ± 254.45% with 0.5 mM H_2O_2 and 1099.05% ± 470.44% with 0.75 mM H_2O_2; two-way ANOVA; $P = 0.0137$; $n = 3$) compared with nontreated cultures (Fig. 3B). Moreover, daily supplementation of porcine TM cells with SIH (10 μM), a membrane-permeant iron chelator, caused a significant reduction in the increased iROS production resulting from culturing of cells for 2 weeks under 40% O_2 (72.57% ± 21.81% vs. 150.86% ± 4.44%; $P = 0.003$; $n = 3$; Fig. 3C).

We also explored whether FAC-treated cells were more sensitive to the cytotoxic effects of H_2O_2. For this, FAC-treated cells were exposed to a bolus dosage of H_2O_2, and cell viability and cytotoxicity were assayed at 3 hours after treatment. As shown in Figure 3D, exogenously added FAC significantly ex-

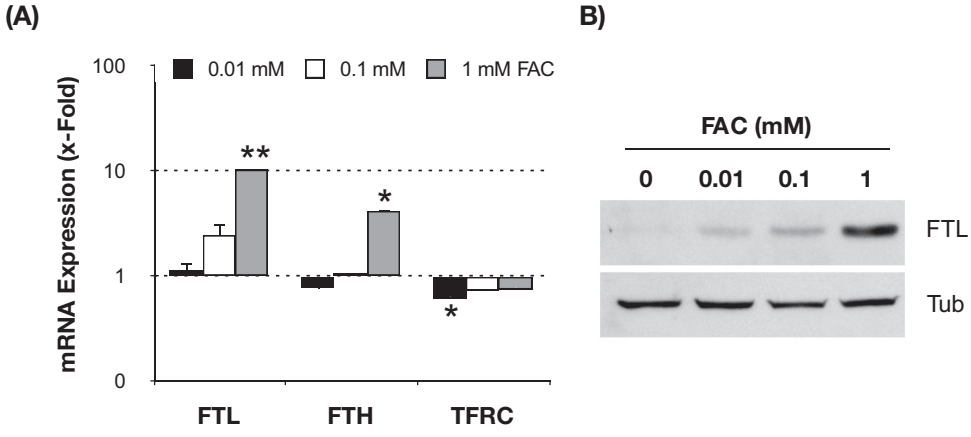

FIGURE 2. Expression levels of genes involved in intracellular iron homeostasis in TM cells supplemented with increasing concentrations of FAC for 3 days. (**A**) Relative mRNA expression levels quantified by qPCR compared with nontreated cells. Values represent mean ± SD. $^*P < 0.05$; $^{**}P < 0.005$; $n = 3$. (**B**) Representative Western blot of FTL protein levels with increasing concentrations of FAC.

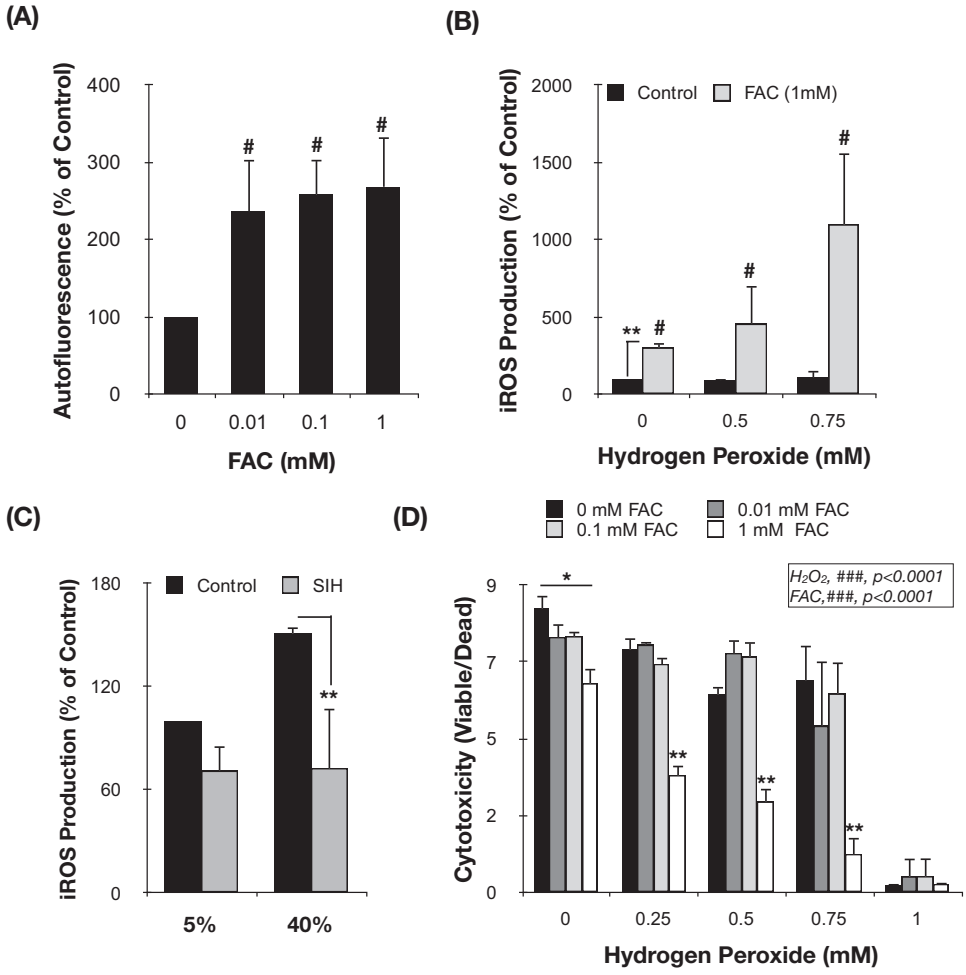

FIGURE 3. Iron increases ROS production and enhanced sensitivity of TM cells to H_2O_2. (**A**) Lipofuscin content in TM cells supplemented for 3 days with increasing concentrations of FAC represented as a percentage of nontreated controls. (**B**) Percentage of increase in iROS production in TM cells supplemented for 24 hours with increasing concentrations of FAC and challenged for 1 hour to a bolus dose of H_2O_2 compared with nontreated controls. (**C**) iROS production in TM cells cultured either at 5% O_2 or at 40% O_2 environment daily treated with SIH (10 μM). Data are represented as a percentage of 5% nontreated control. (**D**) Levels of viability in TM cells supplemented for 24 hours with FAC and challenged for 3 hours to H_2O_2. Data are represented as the ratio between viable and dead cells. Values represent mean ± SD. $^*P < 0.05$; $^{**}P < 0.005$; $n = 3$ (*t*-test). $\#P < 0.05$; $\#\#\#P < 0.0001$ (ANOVA).

acerbated the cytotoxic effects of H_2O_2 in porcine TM cells in a dosage-dependent manner (two-way ANOVA; $P < 0.0001$; $n = 3$).

Intralysosomal Iron Chelation Inhibits Constitutive and Inducible iROS Production and Protects Cultured Porcine TM Cells from H_2O_2-Induced Cytotoxicity

Because of the autophagic degradation of ferritin and other ferruginous material, including mitochondria and metalloproteinases, the lysosomal compartment is the cellular organelle in which most intracellular iron is accumulated. Given the acidic lysosomal pH and the high reducing conditions, most of the iron is found in its redox active form (Fe^{2+}), which can participate in Fenton reactions in the presence of H_2O_2 diffusing into the lysosomes.[15,29] To investigate the potential role of intralysosomal iron in the cytotoxic effect of H_2O_2 in porcine TM cells, we used the lysosomal iron chelator DFO. DFO is a nonmembrane-permeant compound that is taken up into cells by endocytosis and is compartmentalized within the lysosomes, whereby it specifically chelates intralysosomal iron.[36] Primary cultures of porcine TM cells were preincubated for 2 hours with increasing concentrations of DFO (0.05 mM, 0.1 mM, and 0.5 mM) and then exposed to a bolus dosage of H_2O_2 (0 mM, 0.25 mM, 0.5 mM, 0.75 mM, and 1 mM). Viability and cytotoxicity were determined at 3 hours after H_2O_2 treatment. As represented in Figure 4A, H_2O_2 induced a significant decrease in the ratio of viable cells compared with control cultures (ANOVA; $P < 0.0001$; $n = 3$). Although DFO alone did not have any effect on cell viability at the time tested, intralysosomal iron chelation significantly protected porcine TM cells against H_2O_2-induced cell death in a concentration-dependent manner (Figs. 4A, 4C; ANOVA; $P < 0.001$; $n = 3$). Preincubation with DFO also reduced the constitutive FTL protein levels and completely blocked the induction of FTL expression by H_2O_2 treatment (Fig. 4B), analyzed by Western blot analysis at 24 hours after treatment. Moreover, intralysosomal iron chelation caused a statistically significant reduction in the constitutive and in the H_2O_2- (ANOVA; $P < 0.001$; $n = 3$) and FAC-induced iROS production (ANOVA; $P < 0.0001$; $n = 3$; Fig. 4D). These results indicate a key role of lysosomal iron and iROS formation in the molecular mechanisms accompanying H_2O_2-induced cell death in porcine TM cells.

Intralysosomal Iron Chelation Protects Primary Cultures of Porcine TM Cells against Apoptosis and H_2O_2-Induced DNA Fragmentation

Cell death by apoptosis is one of the mechanisms by which H_2O_2 causes cell cytotoxicity. Given that an increasing number of studies in different cell types have recently supported a crucial function of lysosomes in triggering apoptosis,[37] we were interested in investigating whether the chelation of intralysosomal iron was protecting TM cells from undergoing H_2O_2-induced programmed cell death. Apoptosis was detected by monitoring two different parameters: changes in cell membrane permeabilization using YO-PRO/PI dual staining and DNA fragmentation.

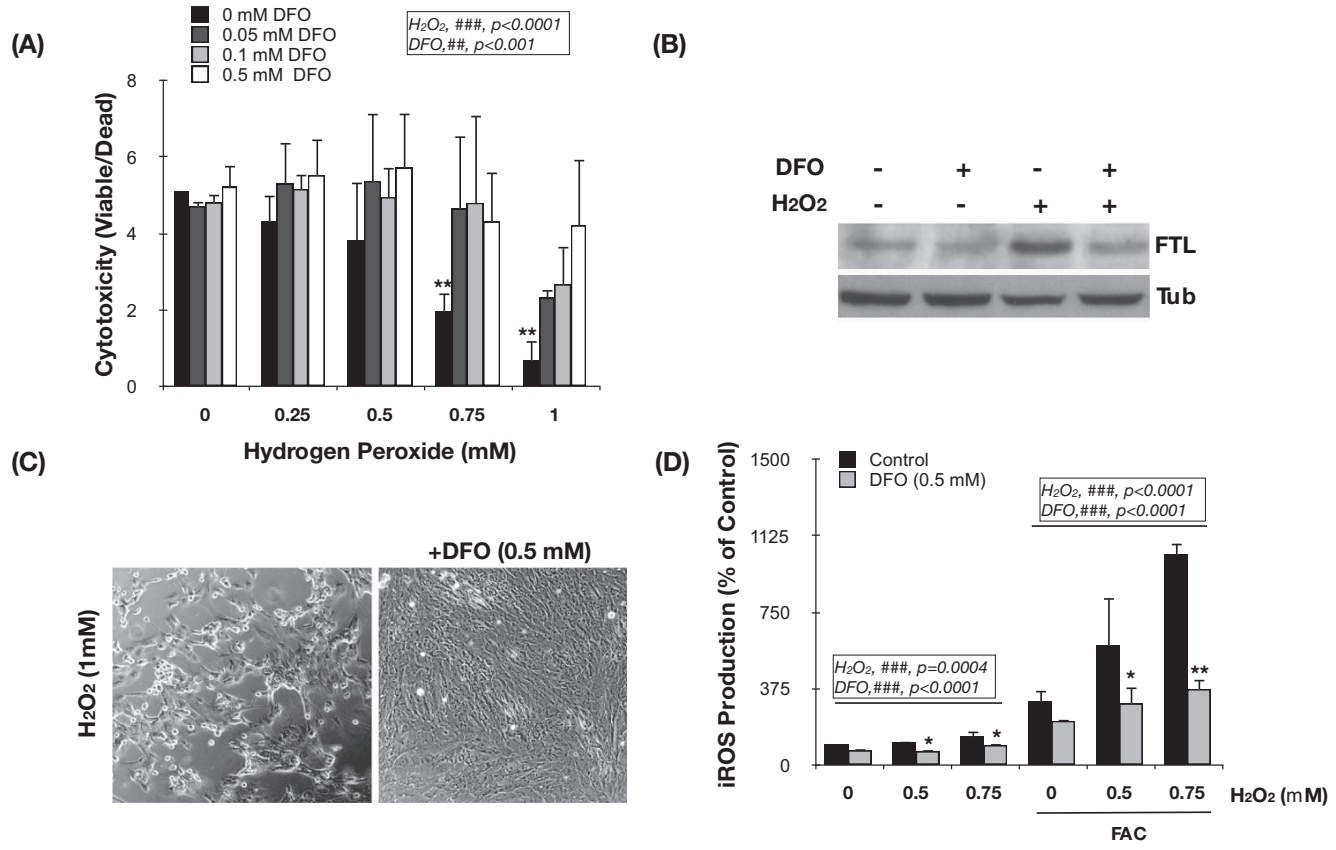

Figure 4. Intralysosomal iron chelation protects TM cells against H_2O_2-induced iROS production and cell death. (**A**) Viability levels of TM cells treated for 2 hours with DFO and challenged for 3 hours to a bolus dosage of H_2O_2. Data are represented as the ratio between viable and dead cells. *Compares effect of H_2O_2. #Compares DFO effect. (**B**) Protein levels of FTL, assayed by Western blot analysis, in TM cells treated with H_2O_2 (0.75 mM) for 24 hours in the absence or presence of DFO (0.5 mM). (**C**) Light microscopy of TM cells incubated for 24 hours with H_2O_2 in the absence (*left*) or presence (*right*) of DFO. (**D**) iROS production in TM cells incubated for 24 hours with FAC (1 mM) and challenged to H_2O_2 in the absence or presence of DFO. Values represent mean ± SD. $^*P < 0.05$; $^{**}P < 0.005$; $n = 3$ (*t*-test). $^{\#\#\#}P < 0.0001$ (ANOVA).

Exposure of porcine TM cells to H_2O_2 triggered both necrosis (identified as $PI^+/YO\text{-}PRO^-$ cells) and early apoptosis ($YO\text{-}PRO^+/PI^-$ cells) in a dosage-dependent manner (ANOVA; $P < 0.0001$; $n = 3$; Fig. 5A). Whereas both events were found to occur in the same proportion in the cells treated with 0.5 mM H_2O_2 (398.93% ± 24.78% and 436.17% ± 73.38% increased in apoptotic and necrotic cells, respectively, compared with nontreated cells), higher concentrations of H_2O_2 (0.75 mM) slightly shifted the balance toward necrosis (3677.91% ± 841.68% increased in $PI^+/YO\text{-}PRO^-$ cells vs. 1821.82% ± 362.31% increased in $YO\text{-}PRO^+/PI^-$ cells). We also observed an increase in the number of cells permeable to both dyes ($YO\text{-}PRO^+/PI^+$, 661.51% ± 152.36%), representing dead cells or cells in the late phase of apoptosis. Preincubation of cultures with DFO before H_2O_2 treatment significantly protected the cells, both against necrosis (3677.91% ± 841.68% compared with 1012.31% ± 127.95% in DFO-treated cells; $P = 0.006$; $n = 3$; 0.75 mM H_2O_2) and early apoptosis (1821.82% ± 362.31% compared with 220.37% ± 53.21% in DFO-treated cells; $P = 0.001$; $n = 3$; 0.75 mM H_2O_2).

DNA fragmentation induced by H_2O_2 was evaluated using the single-cell electrophoresis assay (Comet Assay Kit; Trevigen). As observed in Figures 5B and 5C, treatment of porcine TM cells with H_2O_2 (0.25 mM, 1 hour) induced extensive damage to DNA, visualized by the appearance of a comet tail containing small DNA fragments that migrate from the intact DNA head (2873.04 ± 783.85 compared with 19,678.76 ± 3,617.93 comet area pixels; $P = 0.0001$; $n = 50$). Extension of the DNA damage was significantly reduced when cultures were preincubated with DFO (0.5 mM) before oxidative challenge (9,869.03 ± 5,268.43 pixels in H_2O_2-DFO–treated cells compared with 19,678.76 ± 3,617.93 pixels in H_2O_2-treated cells; $P = 0.001$; $n = 50$).

Intralysosomal Iron Chelation Protects Cultured Porcine TM Cells from H_2O_2-Induced Lysosomal Membrane Permeabilization

To test the potential role of intralysosomal redox-active iron in lysosomal permeabilization due to potential peroxidation induced by lysosomal ROS, we evaluated the integrity of the lysosomal membrane in H_2O_2-treated cells and the potential protective effect of DFO using the LTR-uptake and the AO-relocation methods.

LTR is a lysosomotropic fluorescent dye that accumulates within intact lysosomes, yielding red fluorescence. Rupture of the lysosomal membrane leads to the leakage of the probe into the cytosol, resulting in the appearance of cells with weak red fluorescence (pale cells) that could be detected with fluorescence microscopy (Fig. 6A, arrows indicate cells with lower punctate red staining) and quantified by flow cytometry (Figs. 6B, 6C). As shown in Figures 6A to 6C, exposure of porcine TM cells to H_2O_2 for 3 hours promoted the appearance of pale cells in a concentration-dependent manner (ANOVA; $P = 0.014$; $n = 3$). Lysosomal labilization in response to H_2O_2 was further exacerbated if cells were preloaded with FAC (1 mM) for 24 hours before H_2O_2 treatment. In contrast, preincubation with DFO (0.5 mM) before H_2O_2 treatment significantly caused a

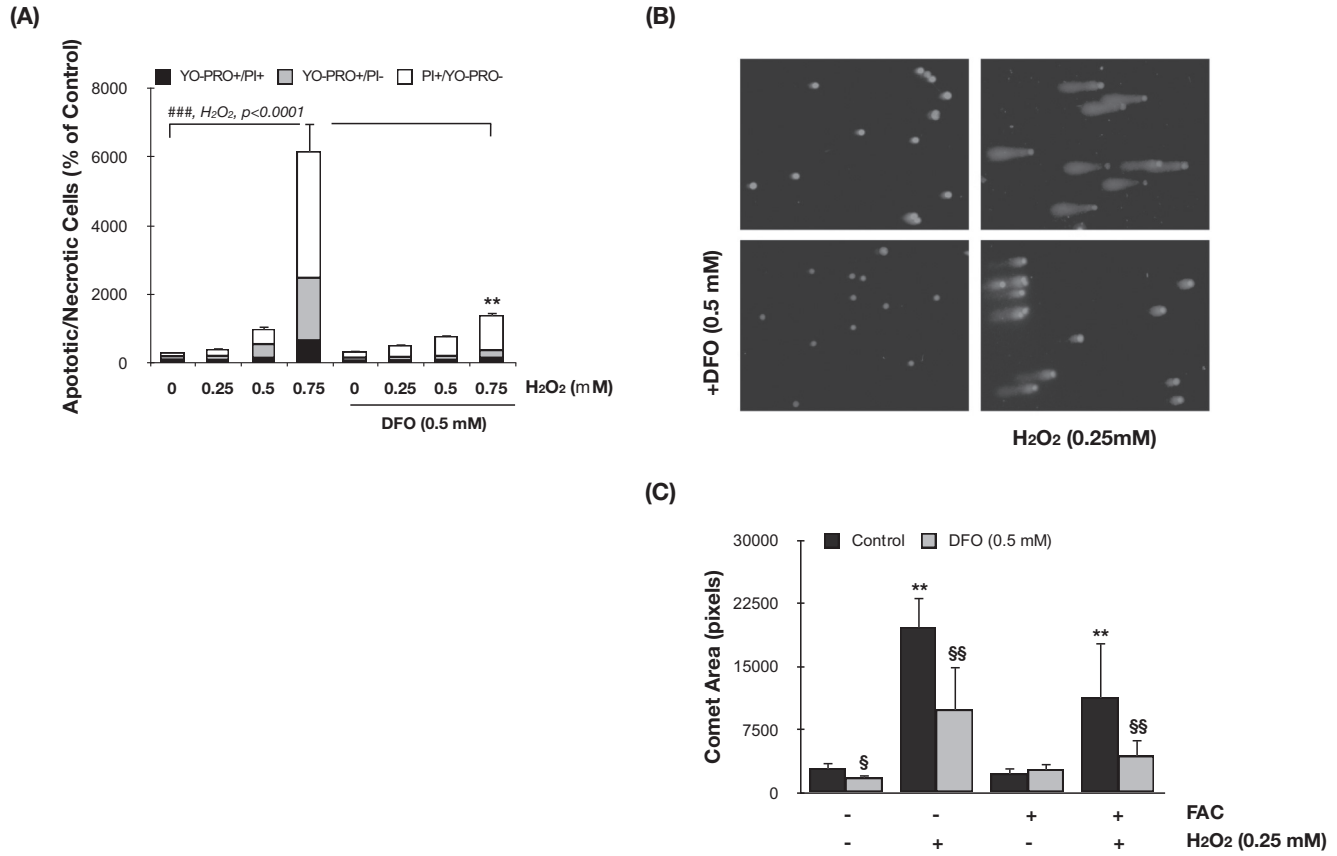

FIGURE 5. Intralysosomal iron chelation protects TM cells against H_2O_2-induced apoptosis and DNA fragmentation. (**A**) Percentage of apoptotic and necrotic cells in TM cells treated for 3 hours with H_2O_2 in the absence or presence of DFO compared with nontreated control cultures. (**B**) Representative image of DNA fragmentation analyzed by assay in TM cells preincubated or not preincubated with DFO and treated for 1 hour with H_2O_2. (**C**) Assay area was scored. Values represent mean ± SD. §$P < 0.05$; **·§§$P < 0.005$. *Compares effect of H_2O_2. §Compares the effect of DFO; $n = 3$ (*t*-test). ###$P < 0.0001$ (ANOVA).

reduction in the number of pale cells (non-FAC treated: ANOVA, $P = 0.0026$, $n = 3$; FAC-treated: ANOVA, $P = 0.0055$, $n = 3$). Similar results were obtained when we quantified LMP by monitoring the relocation of AO, a more sensitive technique. AO is a lysosomotropic metachromatic dye that yields red fluorescence when it accumulates within the lysosomes and green fluorescence when diffuses into the cytosol and nuclei. Lysosomal rupture is detected in this case by an increase in the mean green fluorescence value (Fig. 6D). Altogether, these results support a crucial role of intralysosomal iron in lysosomal permeabilization in porcine TM cells.

Cytosolic Release of Cathepsin D Is Involved in H_2O_2-Induced Cell Death in Porcine TM Cells

One of the potential consequences of lysosomal rupture is the release of lysosomal enzymes into the cytosolic compartment, where they can initiate proteolytic events triggering apoptosis and cell death. To monitor whether H_2O_2 exposure was inducing the translocation of cathepsins into the cytosol, we used BODIPY FL-pepstatin A, a pH-dependent fluorescent probe that binds to CTSD. In control cells, pepstatin A BODIPY FL-cathepsin D complexes were localized, as expected, in the perinuclear region (Fig. 7A, punctate green fluorescence staining). Cells treated with H_2O_2 showed a more diffuse pattern distribution and a decrease in green fluorescence, suggesting the loss of CTSD from the lysosomes in response to H_2O_2. Preincubation with DFO before oxidative challenge completely prevented the relocation of CTSD.

To investigate the potential participation of lysosomal enzymes in H_2O_2-induced cell death, porcine TM cells were pretreated with either leupeptin (0.1 mM, a cysteine proteinase inhibitor) or pepstatin A (0.1 mM, an inhibitor of the aspartic protease cathepsin D) for 30 minutes and then were exposed to a bolus dosage of H_2O_2 (0.75 mM). Cell death was evaluated by quantification of the LDH released to the culture media at 3 hours after treatment. Chemical inhibition of CTSD significantly produced a decrease in the amount of released LDH (0.130 ± 0.025 ROU in pepstatin A/H_2O_2-treated cells vs. 0.427 ± 0.051 ROU in H_2O_2-treated cultures; $P = 0.0008$; $n = 3$; Fig. 7B). Similar results were obtained with a lower dosage of the inhibitor (0.01 mM, data not shown). In contrast, chemical inhibition of cysteine proteinases did not show any protective effect against H_2O_2-induced cell death.

To confirm these results, we generated plasmids containing microRNA sequences to specifically knock down the expression of porcine CTSB or porcine CTSD (Fig. 7D). As shown in Figure 7C, silencing CTSD expression significantly decreased the release of LDH after H_2O_2 treatment (0.366 ± 0.08 ROU vs. 0.614 ± 0.06; $P = 0.016$; $n = 3$).

Resistance of Porcine TM Cells Grown under Hyperoxic Conditions to H_2O_2-Induced Cell Death

We have recently reported lower lysosomal enzyme activity per lysosomal enzyme content in cultured TM cells grown under 40% O_2 compared with cells grown under physiological oxygen concentrations.[30] Considering the previous results, we

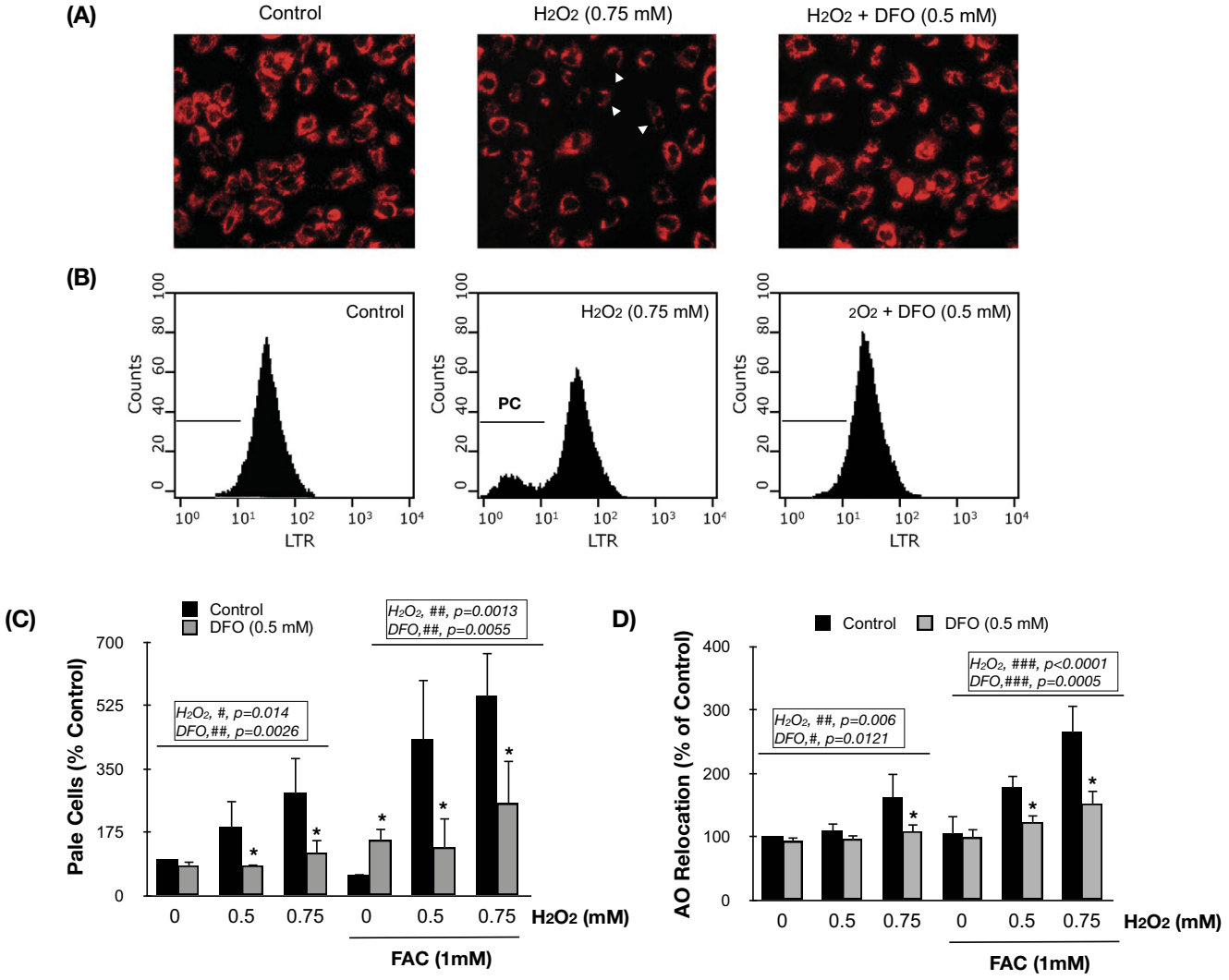

FIGURE 6. Intralysosomal iron chelation protects TM cells against H_2O_2-induced LMP. Representative fluorescence microscopy (**A**) and flow cytometry (**B**) image of TM cells showing the protection of DFO against LMP, identified as cells with decreased LTR red fluorescence (pale cells) using the LTR uptake technique. (**C**) Percentage of pale cells quantified by flow cytometry using the LTR uptake technique compared with nontreated control. (**D**) LMP evaluated by the percentage of increase in mean green fluorescence, quantified by flow cytometry, compared with nontreated control using the AO relocation technique. Values represent mean ± SD. $^*P < 0.05$; $n = 3$ (*t*-test). $\#P < 0.05$; $\#\#P < 0.001$; $\#\#\#P < 0.0001$ (ANOVA).

were interested in evaluating the resistance of these stressed cells against further acute oxidative insult. For this, confluent cultures of porcine TM cells were grown for 2 weeks at either 5% O_2 or 40% O_2 conditions and then were challenged with a bolus dosage of H_2O_2. LDH released to the culture media was quantified at 3 hours after treatment. As observed in Figure 8, cells grown at 40% O_2 demonstrated lower concentrations of LDH in response to H_2O_2, indicating higher resistance to H_2O_2-induced cell death (ANOVA; $P < 0.0001$; $n = 3$).

DISCUSSION

Increasing evidence shows that oxidative stress and free radical damage in the outflow pathway may underlie the pathogenesis of ocular hypertension in glaucoma. The data presented here show that chronic oxidative stress alters intracellular iron homeostasis in human and porcine TM cells, resulting in the accumulation of redox-active iron within TM cells; that intracellular accumulation of iron, in particular within the lysosomal compartment, is accountable for the increase in ROS production observed in the oxidatively stressed cultures; and that lysosomal iron may cause lysosomal labilization and CTSD-mediated TM cell death. These findings suggest a novel mechanism by which oxidative stress might contribute to the pathophysiology of the outflow pathway in glaucoma.

Accumulation of iron has been reported in a variety of tissues and has been increasingly implicated in the pathogenesis of aging and disease.[16–20,23,38] Whether the increase in iron with age is a byproduct of normal aging or whether iron itself is involved in the pathogenesis of aging or age-related disorders is still unknown. The molecular basis of age-related iron accumulation also remains unknown. Our studies demonstrated increased ferritin levels and iron content in primary cultures of TM cells subjected to chronic oxidative stress as an in vitro model of aging. Similar results have been reported in primary cultures of human fibroblasts and in umbilical vein endothelial cells during replicative and stress-induced senescence.[14] Interestingly, iron accumulation was not observed in immortalized cells, suggesting that the changes in iron content result from the processes driving cellular senescence.

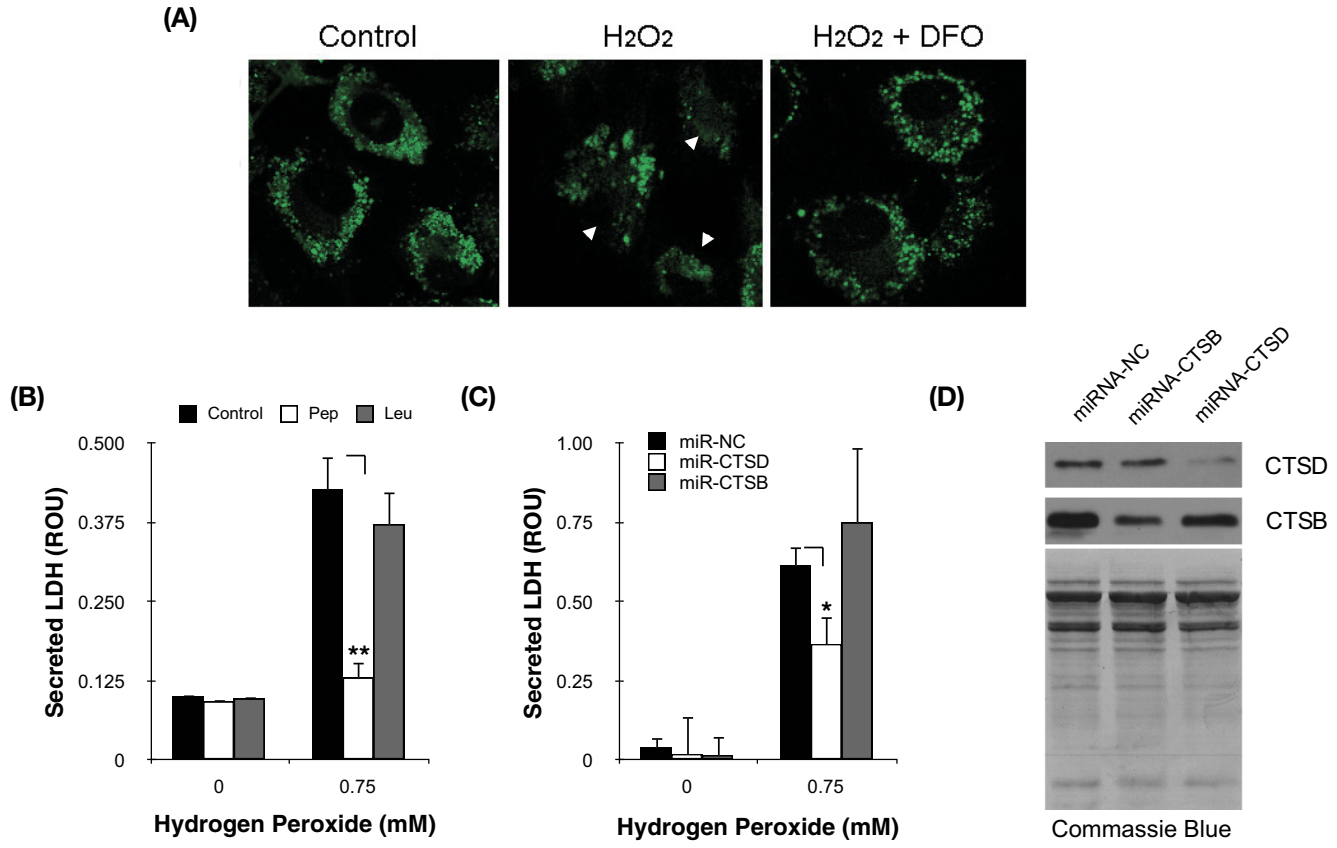

FIGURE 7. Cytosolic CTSD mediates H_2O_2-induced cell death in TM cells. (**A**) Confocal microscopy image showing the localization of CTSD-BODIPY FL-pepstatin A complexes in H_2O_2-treated cells in the absence or presence of DFO. *Arrowheads*: cytosolic localization of complexes. (**B**) Levels of cytotoxicity, quantified by LDH release, in TM cells challenged to H_2O_2 in the presence of leupeptin (0.1 mM) or pepstatin A (0.1 mM). (**C**) Levels of cytotoxicity, quantified by LDH release, in TM cells challenged to H_2O_2 in the presence of constructs expressing microRNA sequences to silence CTSD or CTSB. (**D**) Protein levels of CTSD and CTDB in TM cells nucleofected with miRNA-CTSB or miRNA-CTSD. Total protein levels were evaluated by Coomassie Blue staining. Values represent mean ± SD. $^*P < 0.05$; $^{**}P < 0.005$; $n = 3$.

One plausible mechanism leading to iron accumulation may involve the loss of iron homeostasis at the cellular level. Oxidative stress is known to alter iron homeostasis and to induce an "iron-starved" phenotype in the cells through uncoupling of iron homeostasis and iron uptake mechanisms.[39–41] This may explain our findings that though treatment of TM cells with FAC led, as expected, to decreased levels of TFRC mRNA and to increased FTH and FTL mRNA and proteins levels, porcine and human TM cells exposed to chronic oxidative stress showed a surprising increase in both ferritin and TFRC mRNA levels.

In vitro and in vivo studies have shown that most of the intracellular iron is progressively accumulated within the lysosomal compartment.[15,29] This subcellular localization of iron results from the autophagic degradation of macromolecules and organelles containing iron, including ferritin, metalloproteinases, and mitochondrial electron transport complexes. A major consequence of intralysosomal iron accumulation is its participation in Fenton reactions. Because of the intrinsic low pH and the high reducing conditions in the lysosomal lumen, lysosomal iron is predominantly found in its redox active form, which is able to catalyze the formation of free radicals in the presence of H_2O_2. The intralysosomally generated ROS have been implicated in the formation of lipofuscin, an autofluorescent, polymeric, nondegradable material composed of peroxidized lipids, proteins, and metals and found to progressively accumulate within lysosomes in aging postmitotic cells.[37,42,43] Accordingly, FAC-treated TM cells displayed increased lipofuscin content, iROS production, and enhanced cytotoxicity to H_2O_2. In addition, specific chelation of lysosomal iron using DFO, a nonpermeant iron chelator that is uptaken by endocytosis and therefore is compartmentalized in the lysosomes,[36] reduced both the endogenous radicals and the production of free radicals in the presence of H_2O_2. Furthermore, treatment of TM cells with the membrane-permeant iron chelator SIH significantly blocked the observed production of iROS in TM cells grown in a 40% O_2 environment. All these data confirmed the central role of intralysosomal iron in iROS production. Although SIH specifically chelates not only lysosomal iron but also redox active iron throughout the cell, Kurtz et al.[29] recently demonstrated that the protective effect of SIH against oxidative damage is mediated by lysosomal stabilization. Notably, in contrast to DFO, which triggers cell death by iron starvation during long-term treatment, TM cells supplemented with SIH each day for 2 weeks did not show any sign of cytotoxicity (data not shown).

Along with preventing ROS formation, we found that intralysosomal iron chelation with DFO completely protected the cells against H_2O_2-induced DNA fragmentation and cell death (necrosis and apoptosis). Although mitochondria and caspases have been long considered the master regulators of apoptosis, an increasing number of studies published during the past few years have reported a key role of lysosomes in the early events, triggering both apoptosis and necrosis in response to different stimuli, oxidative stress among them.[37,42,44–48] The continuous iron-catalyzed formation of ROS within lysosomes may promote peroxidation of the lysosomal membrane and lysosomal labilization, with the conse-

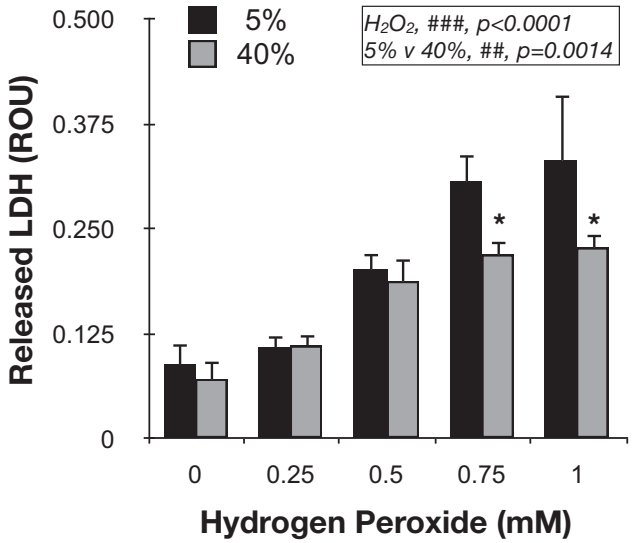

FIGURE 8. Resistance of chronically stressed TM cells to acute oxidative challenge. Levels of cytotoxicity, quantified by LDH release, in TM cells grown for 2 weeks at either 5% O_2 or 40% O_2 challenged for 3 hours to a bolus dosage of H_2O_2. Values represent mean ± SD. $^*P < 0.05$; $n = 3$ (*t*-test). $^{\#\#}P < 0.001$, $^{\#\#\#}P < 0.0001$ (ANOVA).

quent leak and relocation of lysosomal contents into the cytosol, including ROS, iron, and lysosomal enzymes.[29,37,49] Our results showed that, effectively, short-term treatment with a bolus dosage of H_2O_2 induced LMP and the cytosolic release of CTSD in TM cells. Moreover, though rupture of the lysosomal membrane was exacerbated in FAC-treated cells, DFO completely prevented LMP and the relocation of CTSD. Together these findings indicated that the cytoprotective effect observed with the iron chelator in TM cells subjected to oxidative insult involved stabilization of the lysosomal membrane mediated by inhibition of lysosomal ROS production. Interestingly, iron did not affect lysosomal integrity, suggesting that the antioxidant cellular systems are able of coping with the free radicals generated under normal physiological conditions.

Western blot analysis revealed increased levels of FTL after H_2O_2 treatment that were restored with DFO. Because FTL expression is transcriptionally regulated by oxidative stress and is posttranscriptionally regulated through iron,[50] we could not discern with the available data whether such FTL increase was caused by the presence of cytosolic redox active iron leaked from lysosomal rupture, ROS, or both. Similarly, DNA fragmentation might have resulted from the diffusion of iron or ROS to the nucleus or from the activation of nucleases in response to apoptotic signaling. Of particular interest is the upregulation of pyrin, a nuclear iron-binding protein of still unknown function,[51] in human TM cells grown under 40% O_2 conditions.

Cathepsins are the most abundant lysosomal proteases. Both pharmacologic inhibition using pepstatin A and silencing of CTSD expression by miRNA demonstrated a role of the aspartic protease CTSD in H_2O_2-induced cell death in TM cells. This is consistent with the lysosomal-mitochondrial axis theory that suggests lysosomal permeabilization might be an integral part of both the intrinsic and the extrinsic apoptotic pathways and that the synergistic action of lysosomal hydrolases and caspases are necessary for apoptosis.[42] Even though cathepsins are optimally active at acidic pH, they show a residual activity at neutral pH. Acidification of cytosol during apoptosis may help stabilize and prolong their lifetime and thus enable them to cleave cytosolic substrates.[52,53] In particular, CTSD and CTSB have been reported to cleave members of the Bcl2 family, such as Bid and Bax.[46,47,54,55]

A corollary question arising from the data presented here is why, despite the increase in iROS production and increased chelatable iron content, TM cells cultured at 40% O_2 show no signs of cytotoxicity. Furthermore, exposure of TM cells to chronic oxidative stress preconditioned and protected the cells against acute oxidative insult. One possible explanation is that chronic exposure to mild oxidative stress might induce protective mechanisms. In this regard, stressed cultures demonstrated upregulated expression of MT1A, a protein recently reported to protect against lysosomal destabilization and to provide enhanced cellular resistance to oxidative stress.[35] Our previous work demonstrated decreased cathepsin activities per total protein in TM cells grown under 40% O_2 conditions. In view of these findings, it is tempting to speculate that such diminished cathepsin activities might somehow protect the cells against LMP and form part of the antioxidant cellular response. We are conducting studies aimed at determining the integrity of the lysosomes in TM cells cultured in 40% O_2 and whether both these events are related.

The development and progression of glaucoma have long been associated with cumulative oxidative damage in the outflow pathway tissue. A recent study has shown that TM cells have the highest oxygen consumption and that the outflow pathway is the most sensitive tissue to oxidative radicals in the anterior chamber of the eye.[56] Although an increase in chelatable iron content in the human glaucomatous outflow pathway has yet to be proven, our present study shows upregulated FTL mRNA levels and a slight decrease in CP mRNA levels in GTM-3 compared with NTM-5. In addition, microarray analysis showed that, similar to what was found in oxidatively stressed cultures, TM tissue from glaucoma donors demonstrated downregulated and upregulated expression levels of CP and TFRC, respectively.[34] Interestingly, elevated iron content in the angle region has been described in ceruloplasmin/hephaestin double-knockout mice.[57]

Several groups have consistently reported a decrease in cellularity and absolute cell number in the trabecular outflow pathway with aging and in glaucoma.[58–63] This exponential decrease in cellularity in TM cells is similar to that of other aging tissues in which cells are thought not to undergo extensive cell division, such as neurons and skeletal muscle.[61] In addition, a recent work has detected an accumulation of apoptotic cells in the trabecular meshwork of glaucoma donors.[63] Yet the mechanisms leading to TM cell death with aging and in glaucoma remain unknown.

Here we propose that the generation of intralysosomal ROS may induce lysosomal membrane permeabilization and release of CTSD into the cytosol, with consequent TM cell death. Moreover, our data suggest that chelation of lysosomal iron might represent a novel therapeutic strategy to counteract the effect of oxidative stress in aging and in disease.

Acknowledgments

The authors thank Thusita R. Dissanayake (Flow Cytometry Facility, Duke University) for extraordinary help in the flow cytometry analyses.

References

1. Leske MC, Wu S-Y, Hennis A, Honkanen R, Nemesure B, Group BS. Risk factors for incident open-angle glaucoma: the Barbados Eye Studies. *Ophthalmology*. 2008;115:85–93.
2. Ziangirova GG, Antonova OV. [Lipid peroxidation in the pathogenesis of primary open-angle glaucoma]. *Vestn Oftalmol*. 2003;119:54–55.
3. Saccà SC, Pascotto A, Camicione P, Capris P, Izzotti A. Oxidative DNA damage in the human trabecular meshwork: clinical correla-

tion in patients with primary open-angle glaucoma. *Arch Ophthalmol*. 2005;123:458–463.
4. He Y, Leung KW, Zhang Y-H, et al. Mitochondrial complex I defect induces ROS release and degeneration in trabecular meshwork cells of POAG patients: protection by antioxidants. *Invest Ophthalmol Vis Sci*. 2008;49:1447–1458.
5. Izzotti A, Saccà SC, Cartiglia C, De Flora S. Oxidative deoxyribonucleic acid damage in the eyes of glaucoma patients. *Am J Med*. 2003;114:638–646.
6. Zanon-Moreno V, Marco-Ventura P, Lleo-Perez A, et al. Oxidative stress in primary open-angle glaucoma. *J Glaucoma*. 2008;17:263–268.
7. Kumar DM, Agarwal N. Oxidative stress in glaucoma: a burden of evidence. *J Glaucoma*. 2007;16:334–343.
8. Saccà SC, Izzotti A. Oxidative stress and glaucoma: injury in the anterior segment of the eye. *Prog Brain Res*. 2008;173:385–407.
9. Kruszewski M. Labile iron pool: the main determinant of cellular response to oxidative stress. *Mutat Res*. 2003;531:81–92.
10. Salahudeen AA, Bruick RK. Maintaining mammalian iron and oxygen homeostasis: sensors, regulation, and cross-talk. *Ann N Y Acad Sci*. 2009;1177:30–38.
11. MacKenzie EL, Iwasaki K, Tsuji Y. Intracellular iron transport and storage: from molecular mechanisms to health implications. *Antioxid Redox Signal*. 2008;10:997–1030.
12. Eisenstein RS, Blemings KP. Iron regulatory proteins, iron responsive elements and iron homeostasis. *J Nutr*. 1998;128:2295–2298.
13. Killilea DW, Wong SL, Cahaya HS, Atamna H, Ames BN. Iron accumulation during cellular senescence. *Ann N Y Acad Sci*. 2004; 1019:365–367.
14. Killilea DW, Atamna H, Liao C, Ames BN. Iron accumulation during cellular senescence in human fibroblasts in vitro. *Antioxid Redox Signal*. 2003;5:507–516.
15. Meguro R, Asano Y, Odagiri S, Li C, Shoumura K. Cellular and subcellular localizations of nonheme ferric and ferrous iron in the rat brain: a light and electron microscopic study by the perfusion-Perls and -Turnbull methods. *Arch Histol Cytol*. 2008;71:205–222.
16. Loh A, Hadziahmetovic M, Dunaief JL. Iron homeostasis and eye disease. *Biochim Biophys Acta*. 2009;1790:637–649.
17. Chen H, Liu B, Lukas TJ, Suyeoka G, Wu G, Neufeld AH. Changes in iron-regulatory proteins in the aged rodent neural retina. *Neurobiol Aging*. 2009;30:1865–1876.
18. Hahn P, Song Y, Ying G-s, He X, Beard J, Dunaief JL. Age-dependent and gender-specific changes in mouse tissue iron by strain. *Exp Gerontol*. 2009;44:594–600.
19. Aquino D, Bizzi A, Grisoli M, et al. Age-related iron deposition in the basal ganglia: quantitative analysis in healthy subjects. *Radiology*. 2009;252:165–172.
20. Altamura S, Muckenthaler MU. Iron toxicity in diseases of aging: Alzheimer's disease, Parkinson's disease and atherosclerosis. *J Alzheimers Dis*. 2009;16:879–895.
21. Seo AY, Xu J, Servais S, et al. Mitochondrial iron accumulation with age and functional consequences. *Aging Cell*. 2008;7:706–716.
22. Xu J, Knutson MD, Carter CS, Leeuwenburgh C. Iron accumulation with age, oxidative stress and functional decline. *PLoS ONE*. 2008; 3:e2865.
23. Brewer GJ. Risks of copper and iron toxicity during aging in humans. *Chem Res Toxicol*. 2010;23:319–326.
24. Peng J, Peng L, Stevenson FF, Doctrow SR, Andersen JK. Iron and paraquat as synergistic environmental risk factors in sporadic Parkinson's disease accelerate age-related neurodegeneration. *J Neurosci*. 2007;27:6914–6922.
25. Altun M, Edström E, Spooner E, et al. Iron load and redox stress in skeletal muscle of aged rats. *Muscle Nerve*. 2007;36:223–233.
26. Kurz T, Terman A, Gustafsson B, Brunk UT. Lysosomes in iron metabolism, ageing and apoptosis. *Histochem Cell Biol*. 2008;129: 389–406.
27. Dycke C, Charbonnier P, Pantopoulos K, Moulis J-M. A role for lysosomes in the turnover of human iron regulatory protein 2. *Int J Biochem Cell Biol*. 2008;40:2826–2832.
28. Kidane TZ, Sauble E, Linder MC. Release of iron from ferritin requires lysosomal activity. *Am J Physiol, Cell Physiol*. 2006;291: C445–C455.
29. Kurz T, Gustafsson B, Brunk UT. Intralysosomal iron chelation protects against oxidative stress-induced cellular damage. *FEBS Lett J*. 2006;273:3106–3117.
30. Liton P, Lin Y, Luna C, Li G, Gonzalez P, Epstein D. Cultured porcine trabecular meshwork cells display altered lysosomal function when subjected to chronic oxidative stress. *Invest Ophthalmol Vis Sci*. 2008;49:3961–3969.
31. Pang IH, Shade DL, Clark AF, Steely HT, DeSantis L. Preliminary characterization of a transformed cell strain derived from human trabecular meshwork. *Curr Eye Res*. 1994;13:51–63.
32. Helbig H, Hinz JP, Kellner U, Foerster MH. Oxygen in the anterior chamber of the human eye. *Ger J Ophthalmol*. 1993;2:161–164.
33. Cabantchik ZI, Glickstein H, Milgram P, Breuer W. A fluorescence assay for assessing chelation of intracellular iron in a membrane model system and in mammalian cells. *Anal Biochem*. 1996;233: 221–227.
34. Liton PB, Luna C, Challa P, Epstein DL, Gonzalez P. Genome-wide expression profile of human trabecular meshwork cultured cells, nonglaucomatous and primary open angle glaucoma tissue. *Mol Vis*. 2006;12:774–790.
35. Baird SK, Kurz T, Brunk UT. Metallothionein protects against oxidative stress-induced lysosomal destabilization. *Biochem J*. 2006;394:275–283.
36. Lloyd JB, Cable H, Rice-Evans C. Evidence that desferrioxamine cannot enter cells by passive diffusion. *Biochem Pharmacol*. 1991;41:1361–1363.
37. Kurz T, Terman A, Gustafsson B, Brunk UT. Lysosomes and oxidative stress in aging and apoptosis. *Biochim Biophys Acta*. 2008; 1780:1291–1303.
38. Baker JF, Ghio AJ. Iron homoeostasis in rheumatic disease. *Rheumatology*. 2009;48:1339–1344.
39. Bulvik B, Grinberg L, Eliashar R, Berenshtein E, Chevion MM. Iron, ferritin and proteins of the methionine-centered redox cycle in young and old rat hearts. *Mech Ageing Dev*. 2009;130:139–144.
40. Hintze KJ, Theil EC. Cellular regulation and molecular interactions of the ferritins. *Cell Mol Life Sci*. 2006;63:591–600.
41. Caltagirone A, Weiss G, Pantopoulos K. Modulation of cellular iron metabolism by hydrogen peroxide: effects of H_2O_2 on the expression and function of iron-responsive element-containing mRNAs in B6 fibroblasts. *J Biol Chem*. 2001;276:19738–19745.
42. Terman A, Gustafsson B, Brunk UT. The lysosomal-mitochondrial axis theory of postmitotic aging and cell death. *Chem Biol Interact*. 2006;163:29–37.
43. Brunk UT, Terman A. Lipofuscin: mechanisms of age-related accumulation and influence on cell function. *Free Radic Biol Med*. 2002;33:611–619.
44. Turk B, Turk V. Lysosomes as 'suicide bags' in cell death: myth or reality?. *J Biol Chem*. 2009;284:ie10.
45. Baumgartner HK, Gerasimenko JV, Thorne C, et al. Caspase-8-mediated apoptosis induced by oxidative stress is independent of the intrinsic pathway and dependent on cathepsins. *Am J Physiol Gastrointest Liver Physiol*. 2007;293:G296–G307.
46. Blomgran R, Zheng L, Stendahl O. Cathepsin-cleaved Bid promotes apoptosis in human neutrophils via oxidative stress-induced lysosomal membrane permeabilization. *J Leukoc Biol*. 2007;81:1213–1223.
47. Castino R, Bellio N, Nicotra G, Follo C, Trincheri NF, Isidoro C. Cathepsin D-Bax death pathway in oxidative stressed neuroblastoma cells. *Free Radic Biol Med*. 2007;42:1305–1316.
48. Haendeler J, Popp R, Goy C, Tischler V, Zeiher AM, Dimmeler S. Cathepsin D and H_2O_2 stimulate degradation of thioredoxin-1: implication for endothelial cell apoptosis. *J Biol Chem*. 2005;280: 42945–42951.
49. Tenopoulou M, Doulias P-T, Barbouti A, Brunk U, Galaris D. Role of compartmentalized redox-active iron in hydrogen peroxide-induced DNA damage and apoptosis. *Biochem J*. 2005;387:703–710.
50. Tsuji Y, Ayaki H, Whitman SP, Morrow CS, Torti SV, Torti FM. Coordinate transcriptional and translational regulation of ferritin in response to oxidative stress. *Mol Cell Biol*. 2000;20:5818–5827.
51. Pang H, Bartlam M, Zeng Q, et al. Crystal structure of human pirin: an iron-binding nuclear protein and transcription cofactor. *J Biol Chem*. 2004;279:1491–1498.

52. Turk B, Bieth JG, Björk I, et al. Regulation of the activity of lysosomal cysteine proteinases by pH-induced inactivation and/or endogenous protein inhibitors, cystatins. *Biol Chem Hoppe-Seyler*. 1995;376:225–230.
53. Lagadic-Gossmann D, Huc L, Lecureur V. Alterations of intracellular pH homeostasis in apoptosis: origins and roles. *Cell Death Differ*. 2004;11:953–961.
54. Stoka V, Turk B, Schendel SL, et al. Lysosomal protease pathways to apoptosis: cleavage of bid, not pro-caspases, is the most likely route. *J Biol Chem*. 2001;276:3149–3157.
55. Joy B, Sivadasan R, Abraham TE, et al. Lysosomal destabilization and cathepsin B contributes for cytochrome *c* release and caspase activation in embelin-induced apoptosis. *Mol Carcinog*. 2010;49:324–336.
56. Izzotti A, Sacca S, Longobardi M, Cartiglia C. Sensitivity of ocular anterior-chamber tissues to oxidative damage and its relevance to glaucoma pathogenesis. *Invest Ophthalmol Vis Sci*. 2009;50:5251–5258.
57. Hadziahmetovic M, Dentchev T, Song Y, et al. Ceruloplasmin/hephaestin knockout mice model morphologic and molecular features of AMD. *Invest Ophthalmol Vis Sci*. 2008;49:2728–2736.
58. Miyazaki M, Segawa K, Urakawa Y. Age-related changes in the trabecular meshwork of the normal human eye. *Jpn J Ophthalmol*. 1987;31:558–569.
59. Alvarado J, Murphy C, Juster R. Trabecular meshwork cellularity in primary open-angle glaucoma and nonglaucomatous normals. *Ophthalmology*. 1984;91:564–579.
60. Tschumper RC, Johnson DH. Trabecular meshwork cellularity: differences between fellow eyes. *Invest Ophthalmol Vis Sci*. 1990; 31:1327–1331.
61. Alvarado J, Murphy C, Polansky J, Juster R. Age-related changes in trabecular meshwork cellularity. *Invest Ophthalmol Vis Sci*. 1981; 21:714–727.
62. Liton PB, Challa P, Stinnett S, Luna C, Epstein DL, Gonzalez P. Cellular senescence in the glaucomatous outflow pathway. *Exp Gerontol*. 2005;40:745–748.
63. Baleriola J, García-Feijoo J, Martínez-de-la-Casa JM, Fernández-Cruz A, de la Rosa EJ, Fernández-Durango R. Apoptosis in the trabecular meshwork of glaucomatous patients. *Mol Vis*. 2008;14:1513–1516.